

## Virtual photon fragmentation functions

Jianwei Qiu and Xiaofei Zhang

*Department of Physics and Astronomy, Iowa State University, Ames, Iowa 50011*

(Received 2 January 2001; published 4 September 2001)

We introduce operator definitions for virtual photon fragmentation functions, which are needed for reliable calculations of Drell-Yan transverse momentum ( $Q_T$ ) distributions when  $Q_T$  is much larger than the invariant mass  $Q$ . We derive the evolution equations for these fragmentation functions. We calculate the leading order evolution kernels for partons to fragment into an unpolarized as well as a polarized virtual photon. We find that fragmentation functions to a longitudinally polarized virtual photon are most important at small  $z$ , and the fragmentation functions to a transversely polarized virtual photon dominate the large  $z$  region. We discuss the implications of this finding to the  $J/\psi$  mesons' polarization at large transverse momentum.

DOI: 10.1103/PhysRevD.64.074007

PACS number(s): 12.38.Bx, 12.38.Cy, 13.85.Qk, 14.70.Bh

### I. INTRODUCTION

Gluon distribution plays a central role in calculating many important signatures at hadron colliders because of the dominance of gluon initiated subprocesses. A precise knowledge of the gluon distribution is absolutely vital for reliable predictions for signal as well as background cross sections [1]. A great effort has been devoted to finding good physical observables for extracting information on gluon distribution [2,3].

For many years, prompt photon production has been thought of as a clean signal for information on gluon distribution because its cross section at lowest order is dominated by the ‘‘Compton’’ subprocess  $g + q \rightarrow \gamma + q$ , and this dominance is preserved at higher orders [4–7]. However, the theoretical and experimental complications have limited our ability to extract clean information on the gluon distribution from direct photon data [8]. At collider energies, prompt photons are observed and their cross sections are measured only if the photons are relatively isolated in phase space. Isolation is required to reduce various hadronic backgrounds. But at the same time, the cross section is no longer totally inclusive and theoretical predictions become sensitive to the isolation parameters [6,9]. In addition, phenomenological fragmentation functions are needed for including photons emerged from the long-distance fragmentation of quarks and gluons that are themselves produced at short distance [4,7]. Our knowledge on phenomenological fragmentation functions and the theoretical uncertainties associated with the isolation prevent fully quantitative determinations of gluon distribution from the collider data on isolated photons. Although data at fixed target energies provide good information on gluon distribution at large  $x$  [10], the controversy about how much  $k_T$  smearing is required to understand the data introduces the significant uncertainties to the gluon distributions [11,12]. As a result, all direct photon data were excluded from recent CTEQ global analyses of parton distributions [8].

Recently, Berger, Gordon, and Klasen (BGK) showed that Drell-Yan transverse momentum ( $Q_T$ ) distributions in hadronic collisions are dominated by partonic subprocesses initiated by incident gluons if  $Q_T > Q/2$ , where  $Q$  is the invariant mass of the produced lepton pairs [13]. BGK argue that

Drell-Yan  $Q_T$  distribution is an advantageous source of constraints on the gluon distribution, free from the experimental and theoretical complications of photon isolation that beset studies of prompt photon production.

Other than the difference between a virtual and a real photon, Drell-Yan and prompt photon production share the same partonic subprocesses. The virtual photon produced in Drell-Yan process subsequently decays into a pair of leptons. Since we are mainly interested in the cross section at high  $Q_T$  and low  $Q$ , we ignore the  $Z$  channel contributions in this paper. If we integrate over angular dependence of the lepton pairs, the Drell-Yan massive lepton-pair production between hadron  $A$  and  $B$  can be expressed in terms of an inclusive production of a virtual photon [13]:

$$\frac{d\sigma_{AB \rightarrow l^+ l^-}(Q)}{dQ^2 dQ_T^2 dy} = \left( \frac{\alpha_{em}}{3\pi Q^2} \right) \frac{d\sigma_{AB \rightarrow \gamma^*}(Q)}{dQ_T^2 dy}. \quad (1)$$

Because of the advantage of measuring the leptons, Drell-Yan massive lepton-pair production as well as the inclusive virtual photon production defined in Eq. (1) are entirely inclusive. The usual factorization theorems in quantum chromodynamics (QCD) should apply [14,15]:

$$\begin{aligned} \frac{d\sigma_{AB \rightarrow \gamma^*}(Q)}{dQ_T^2 dy} &= \sum_{a,b} \int dx_1 \phi_{a/A}(x_1, \mu) \int dx_2 \phi_{b/B}(x_2, \mu) \\ &\times \frac{d\hat{\sigma}_{ab \rightarrow \gamma^*}(Q)}{dQ_T^2 dy}(x_1, x_2, Q, Q_T, y; \mu), \end{aligned} \quad (2)$$

where  $\Sigma_{a,b}$  run over all parton flavors, the  $\phi_{a/A}$  and  $\phi_{b/B}$  are parton distributions, and  $\mu$  represents both renormalization and factorization scale. In Eq. (2),  $d\hat{\sigma}_{ab \rightarrow \gamma^*}(Q)/dQ_T^2 dy$  are short-distance partonic hard parts and perturbatively calculable to all orders in  $\alpha_s(\mu)$ . Similar to prompt photon production, the lowest order ‘‘Compton’’ subprocess to a virtual photon  $g + q \rightarrow \gamma^* + q$  dominates the  $Q_T$  distributions at large  $Q_T$  as long as the collision energy is high enough to overcome the phase space penalty caused by the virtual photon mass. Therefore, Drell-Yan  $Q_T$  distribution at large  $Q_T$  is an advantageous source of information on the gluon distribution [13].

When  $Q_T$  is very different from  $Q$ , calculating the cross sections for the virtual photon (or the Drell-Yan massive lepton-pair) production is a two-scale problem in QCD perturbation theory. The short-distance partonic parts  $d\hat{\sigma}_{ab\rightarrow\gamma^*(Q)}/dQ_T^2 dy$  in Eq. (2), calculated perturbatively in the conventional fixed-order QCD perturbation theory, receive the large logarithms of the ratio of these two physical scales:  $Q_T$  and  $Q$ . As a result, the high order corrections in powers of  $\alpha_s$  are not necessarily small, and the ratio  $\sigma^{NLO}/\sigma^{LO} [\propto \alpha_s \times (\text{large logarithms})]$  can be larger than 1. Therefore, the convergence of the conventional perturbative expansion in powers of  $\alpha_s$  is impaired, and the logarithms must be resummed.

For example, when  $Q_T \ll Q$ , the Drell-Yan transverse momentum distributions calculated in the fixed-order QCD perturbation theory are known not to be reliable [16]. Only after including the all-order resummation of the large  $\ln(Q^2/Q_T^2)$ , the QCD predictions to the Drell-Yan transverse momentum distributions at  $Q_T \ll Q$  become consistent with the experimental data [17]. Similarly, when  $Q_T \gg Q$ , the perturbatively calculated short-distance partonic parts in Eq. (2) receive one power of the large logarithm  $\ln(Q_T^2/Q^2)$  at every order of  $\alpha_s$  beyond the leading order. Therefore, at sufficiently large  $Q_T$  and  $\sqrt{S}$ , the resummations of such large logarithms are necessary for reliable QCD predictions.

In order to help resumming the large logarithm, we introduce a concept of virtual photon fragmentation functions  $D_{f\rightarrow\gamma^*}(z, \mu_F^2; Q^2)$  for a parton of flavor  $f$  to fragment into a virtual photon of invariant mass  $Q$ . Normally, a virtual particle state is not physical, and therefore, a fragmentation function to such a state may be gauge dependent and ill defined. However, if such a virtual state immediately decays into a *completely* measured physical state, we believe that a fragmentation function to such a virtual state is effectively physical. The fragmentation function is experimentally measurable if the decay to the physical state is calculable.

Unlike the real photon fragmentation functions [4], the virtual photon fragmentation functions are fully perturbative if  $Q \gg \Lambda_{\text{QCD}}$ . Similarly, their spacelike counterpart, virtual photon structure functions, were proved to be perturbative and have been well studied [18,19]. In terms of the virtual photon fragmentation functions, the conventional perturbative expansion for  $d\hat{\sigma}_{ab\rightarrow\gamma^*(Q)}/dQ_T^2 dy$  in Eq. (2) can be *reorganized* according to a new factorization formula such that the large logarithms are resummed to all orders in  $\alpha_s$ . The detailed derivation of the new factorization formula for the virtual photon production at  $Q_T \gg Q$ , which include all order resummations of the large logarithms, will be published elsewhere [20]. In this paper, we concentrate on the process independent physics associated with the virtual photon fragmentation functions.

In the next section, we derive the cut vertex and corresponding operator definitions for virtual photon fragmentation functions. We argue that the virtual photon fragmentation functions are in principle perturbatively calculable to all orders in  $\alpha_s$  if  $Q \gg \Lambda_{\text{QCD}}$ . With an assumption of strong ordering in the fragmenting partons' invariant mass, we derive a set of the evolution equations for these fragmentation

functions. The resummation of large logarithms in powers of  $\alpha_s$  is achieved by solving the evolution equations. We calculate the leading order evolution kernels for these evolution equations. With the calculated evolution kernels, we derive the virtual photon fragmentation functions.

Because of our ability of measuring the leptons, we can probe the polarization of the virtual photon in Drell-Yan massive lepton-pair production. Therefore, it is also physically meaningful to define fragmentation functions to a virtual photon with a specific polarization. In Sec. III, we derive the evolution equations and the leading order evolution kernels to polarized virtual photon fragmentation functions.

In Sec. IV, we present our numerical results for virtual photon fragmentation functions. By showing the fragmentation functions at different scales, we demonstrate the evolution properties of the fragmentation functions for partons to a unpolarized as well as a polarized virtual photon. We find that fragmentation functions to a longitudinally polarized virtual photon are most important at small  $z$ , and the fragmentation functions to a transversely polarized virtual photon dominate the large  $z$  region. When  $Q_T$  is large while  $\sqrt{S}$  is fixed, fragmentation functions at large  $z$  are more relevant for calculating the cross sections. Therefore, we conclude that the virtual photons produced in a unpolarized Drell-Yan massive lepton-pair production are more likely to be transversely polarized at high  $Q_T$ .

Recent data on  $J/\psi$  polarization measured by Collider Detector at Fermilab (CDF) Collaboration at Fermilab Tevatron seem to be inconsistent with the predictions from various models of  $J/\psi$  production [22]. The virtual photon production (extracted from Drell-Yan massive lepton-pair production) at large  $Q_T$  and small  $Q^2$  has a lot in common with the  $J/\psi$  production at high  $Q_T$ . They both have two large physical scales:  $Q_T$  and  $Q^2$ , which is equal to  $M_{J/\psi}^2$  in the case of  $J/\psi$  production; and  $Q_T^2$  is much larger than  $Q^2$ . If the collision energy  $\sqrt{S}$  is large enough and the logarithm  $\ln(Q_T^2/Q^2)$  is so important that the resummed fragmentation contributions dominate the production cross sections, the virtual photon and  $J/\psi$  production will share the *same* partonic subprocesses. Only difference between the virtual photon and  $J/\psi$  production at high  $Q_T$  is the fragmentation functions. The virtual photon fragmentation functions are completely perturbative, while the parton to  $J/\psi$  fragmentation functions involve final-state nonperturbative interactions. Understanding the difference in such final-state interactions is very important for reliable predictions of  $J/\psi$  production. We propose to measure the virtual photon polarization in Drell-Yan massive lepton-pair production at large  $Q_T$  and low  $Q^2$ . Because the virtual photon polarizations in Drell-Yan massive lepton-pair production are completely calculable and independent of the final-state nonperturbative effect, the measurements of the virtual photon polarizations at high  $Q_T$  provide not only a good test of QCD perturbation theory, but also a reference process to test the models of  $J/\psi$  formation.

## II. UNPOLARIZED VIRTUAL PHOTON FRAGMENTATION FUNCTIONS

In this section, we derive the operator definitions for the virtual photon fragmentation functions, and corresponding

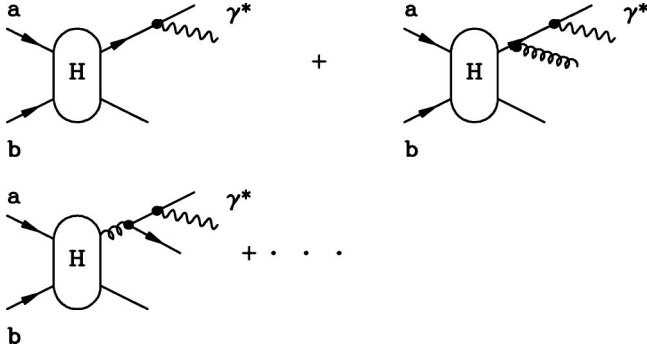


FIG. 1. Sample subprocesses that give the large logarithmic contributions to the cross sections of the virtual photon (or the Drell-Yan massive lepton-pair) production.

evolution equations. We calculate the leading order evolution kernels for the evolution equations and derive the virtual photon fragmentation functions by solving the evolution equations numerically.

### A. Definitions for the virtual photon fragmentation functions

As with other fragmentation functions [23], a virtual photon fragmentation function  $D_{f \rightarrow \gamma^*}(z, \mu_F^2; Q^2)$  is defined as a probability density to find a virtual photon of invariant mass  $Q$  and momentum fraction  $z$  from a parent parton of flavor  $f$ . However, unlike the real photon or single hadron (e.g., pion or proton) fragmentation functions, which are sensitive to the nonperturbative inputs, the virtual photon fragmentation functions defined below depend on only the physics *between* two large momentum scales:  $Q$  and  $\mu_F$  (the fragmentation scale). We argue below that the virtual photon fragmentation functions are completely perturbative if  $Q$  is large enough.

In order to simplify our derivations, we choose a frame in which the virtual photon is moving very fast along the  $z$  axis,

$$Q^\mu = (Q^+, Q^-, \vec{0}_T) \quad \text{and} \quad Q^- = \frac{Q^2}{2Q^+} \quad (3)$$

with  $Q^+ \gg Q^-$ . We also introduce two useful vectors

$$\vec{n}^\mu = (1, 0, \vec{0}_T) \quad \text{and} \quad n^\mu = (0, 1, \vec{0}_T) \quad (4)$$

with  $\vec{n}^2 = n^2 = 0$  and  $\vec{n}^\mu n_\mu = 1$ . For any four-vector  $p$ , we have  $p^\mu \vec{n}_\mu = p^-$  and  $p^\mu n_\mu = p^+$ .

In order to resum the large logarithms for the Drell-Yan massive lepton-pair (or virtual photon) production at large  $Q_T$ , we need to identify where the large logarithms  $[\ln(Q_T^2/Q^2)]^n$  come from, and the pattern of these large logarithmic contributions. In a physical gauge (such as the light-cone gauge), these large logarithms come from the partonic subprocesses, as shown in Fig. 1, in which the virtual photon is produced from the bremsstrahlung of a quark (or an antiquark). The quark (or antiquark) itself was produced either at the hard collision or from the gluon fragmentation. These partonic subprocesses fall into a generic pattern: first, a parton is produced at a very short distance ( $\sim 1/Q_T$ ); then this parton fragments into a number of almost collinear partons

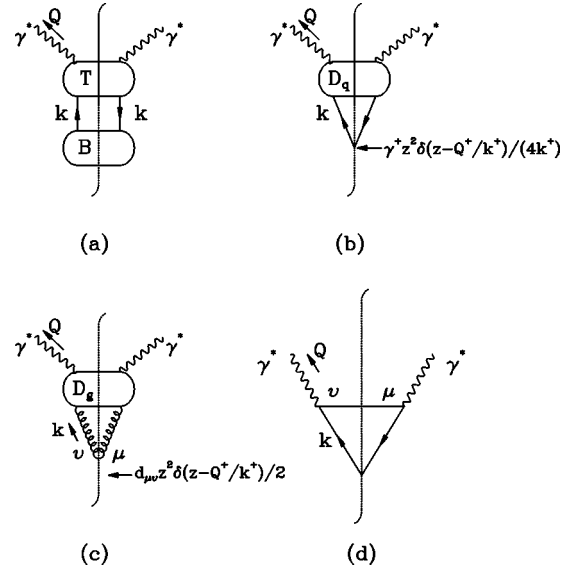


FIG. 2. (a) A generic diagram for a scattering process in which a quark of momentum  $k$  fragments into a virtual photon of invariant mass  $Q$ ; (b) the cut-vertex diagram for quark-to-virtual-photon fragmentation function; (c) the cut-vertex diagram for gluon-to-virtual-photon fragmentation function; (d) the lowest order cut-vertex diagram for a quark to a virtual photon.

(corresponding to the leading logarithmic contributions); and finally, a quark (or an antiquark), which was produced during this fragmentation process, radiates the virtual photon. This generic pattern suggests that the large logarithmic contributions to the virtual photon production can be factorized into two parts: (1) production of a parton at a distance scale  $\sim 1/Q_T$  and (2) fragmentation from the parton to the observed virtual photon, which includes all the leading logarithmic contributions from the distance scale  $1/Q_T$  to  $1/Q$ . The virtual photon fragmentation functions are introduced to represent the physics of the second part.

In order to derive the exact definitions for the virtual photon fragmentation functions, let us first consider a generic quark to virtual photon fragmentation process, as shown in Fig. 2(a). The top part, labeled by  $T$ , corresponds to the fragmentation from a quark of momentum  $k$  to a virtual photon of invariant mass  $Q$ ; and the bottom part, labeled by  $B$ , represents a short-distance hard collision at a scale  $\mu \gg Q$ . By carrying out collinear expansion of the quark momentum  $k$  in the  $B$  at  $k^\mu = (Q^+/z)\vec{n}^\mu$  and separation of the trace between the top and the bottom [24], we factorize the generic fragmentation process as follows:

$$\begin{aligned} & \int \frac{d^4 k}{(2\pi)^4} \text{Tr}[B_q(\mu, k) T_{q \rightarrow \gamma^*}(k, Q)] \\ & \approx \int \frac{dz}{z^2} \text{Tr} \left[ B_q \left( \mu, k = \frac{Q^+}{z} \right) \left\{ \gamma^- \left( \frac{Q^+}{z} \right) \right\} \right] \\ & \quad \times \int \frac{d^4 k}{(2\pi)^4} \text{Tr} \left[ \left\{ \frac{\gamma^+}{4k^+} z^2 \delta \left( z - \frac{Q^+}{k^+} \right) \right\} T_{q \rightarrow \gamma^*}(k, Q) \right] \end{aligned}$$

$$\equiv \int \frac{dz}{z^2} H_q \left( \mu, k = \frac{Q^+}{z} \right) D_{q \rightarrow \gamma^*}(z, \mu_F^2; Q^2), \quad (5)$$

where  $H_q(\mu, k = Q^+/z) \equiv \text{Tr}[B_q(\mu, k = Q^+/z)\{\gamma^-(Q^+/z)\}]$  represents the leading power short-distance production of a quark of momentum  $k^\mu = (Q^+/z)\bar{n}^\mu$  and

$$D_{q \rightarrow \gamma^*}(z, \mu_F^2; Q^2) \equiv \int \frac{d^4 k}{(2\pi)^4} \text{Tr} \left[ \left\{ \frac{\gamma^+}{4k^+} z^2 \delta \left( z - \frac{Q^+}{k^+} \right) \right\} T_{q \rightarrow \gamma^*}(k, Q) \right] \quad (6)$$

is the quark-to-virtual-photon fragmentation function in terms of its cut-vertex definition [25]. As shown in Fig. 2(b),

$$\left\{ \frac{\gamma^+}{4k^+} z^2 \delta \left( z - \frac{Q^+}{k^+} \right) \right\}$$

in Eq. (6) is the corresponding cut vertex. The  $\mu_F$  is a fragmentation scale which is of order  $\sim \mu$  and will be specified below. The cut vertex for an antiquark-to-virtual-photon fragmentation function is the same as that for a quark-to-virtual-photon fragmentation function.

Similarly, by considering a generic gluon to virtual photon fragmentation process, we derive the cut-vertex definition for the gluon-to-virtual-photon fragmentation function with the cut vertex  $\{\frac{1}{2}d^{\mu\nu}z^2\delta(z - Q^+/k^+)\}$ , as shown in Fig. 2(c). The tensor  $d^{\mu\nu}$  is defined as

$$d^{\mu\nu} = -g^{\mu\nu} + \bar{n}^\mu n^\nu + n^\mu \bar{n}^\nu. \quad (7)$$

From the cut-vertex definitions in Figs. 2(b) and 2(c), we derive corresponding operator definitions for the virtual photon fragmentation functions as follows. By representing the diagram in Fig. 1(b) in terms of quark fields, we have

$$D_{q \rightarrow \gamma^*}(z, \mu_F^2; Q^2) = \int \frac{d^4 k}{(2\pi)^4} \left[ z^2 \delta \left( z - \frac{Q^+}{k^+} \right) \frac{1}{4k^+} \right] \times (2\pi)^4 \delta^4 \left( k - Q - \sum_X k_X \right) \prod_X \frac{d^3 k_X}{(2\pi)^3 2E_X} \times \frac{1}{N} \sum_{i=1}^N \text{Tr}[\gamma^+ \langle 0 | \psi_{q_i}(0) | \gamma^*(Q) X \rangle] \times \langle X \gamma^*(Q) | \bar{\psi}_{q_i}(0) | 0 \rangle \quad (8)$$

$$= \frac{z}{4} \int \frac{dy^-}{2\pi} e^{-i(Q^+/z)y^-} \times \frac{1}{N} \sum_{i=1}^N \text{Tr}[\gamma^+ \langle 0 | \psi_{q_i}(0) | \gamma^*(Q) \rangle] \times \langle \gamma^*(Q) | \bar{\psi}_{q_i}(y^-) | 0 \rangle,$$

where  $(1/N)\sum_{i=1}^N$  with  $N=3$  indicates the average over the quark color. Similarly, we derive the operator definition for the gluon-to-virtual-photon fragmentation function:

$$D_{g \rightarrow \gamma^*}(z, \mu_F^2; Q^2) = \frac{z^2}{2Q^+} \int \frac{dy^-}{2\pi} e^{-i(q^+/z)y^-} (-g_{\mu\nu}) \times \frac{1}{N^2-1} \sum_{a=1}^{N^2-1} \langle 0 | F_a^{+\mu}(0) | \gamma^*(Q) \rangle \times \langle \gamma^*(Q) | F_a^{+\nu}(y^-) | 0 \rangle. \quad (9)$$

Both operator definitions in Eqs. (8) and (9) are in the light-cone gauge. Proper insertion of a line integral of the color and electromagnetic potential is needed to make them both color and electromagnetic gauge invariant [23,26]. The operator definitions for the virtual photon fragmentation functions in Eqs. (8) and (9) are almost identical to the definitions of real photon fragmentation functions. However, due to the nonvanishing invariant mass  $Q$ , the real and virtual photon fragmentation functions have very different functional dependence on the momentum fraction  $z$  and fragmentation scale  $\mu_F$ .

Since the photons can directly interact with quarks, both real and virtual photon fragmentation functions can be expressed in terms of the same set of the cut-vertex diagrams, as shown in Fig. 3. Because of the possible collinear divergences when a real photon is parallel to the fragmenting parton, QCD perturbation theory cannot calculate these cut-vertex diagrams reliably to derive the real photon fragmentation functions. As a result, some nonperturbative functions have to be introduced to represent the physics in the collinear region. Consequently, the real photon fragmentation functions are not completely perturbative. On the other hand, the virtual photon's large mass cuts off the collinear region, and therefore, the cut-vertex diagrams in Fig. 3 are free of the collinear divergences when the  $Q$  is finite. Without the collinear divergences, the virtual photon fragmentation functions defined in Eqs. (8) and (9) or equivalently in Fig. 3 are perturbatively calculable.

However, the exact functional forms of the virtual photon fragmentation functions depend on the renormalization conditions that we choose to renormalize the composite operators in Eqs. (8) and (9) or the cut vertices in Fig. 3. Because we renormalize these operators at a distance scale  $1/\mu_F \sim 1/Q_T$ , the differences in the virtual photon fragmentation functions, due to the different renormalization conditions, are of the short distance in nature. Since the virtual photon (or the Drell-Yan massive lepton pair) cross sections at high  $Q_T$  can be systematically factorized, the differences in the virtual

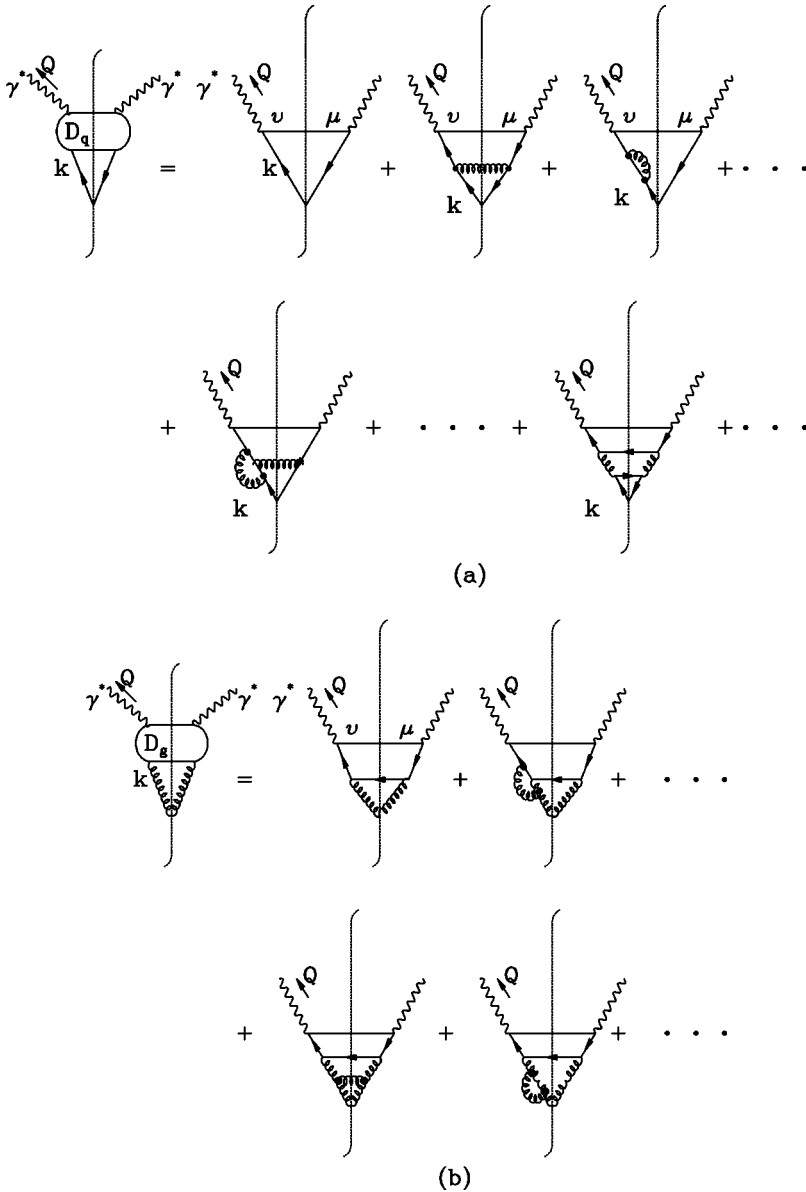


FIG. 3. Sample cut-vertex diagrams that contribute to the quark-to-virtual-photon (a) and the gluon-to-virtual-photon fragmentation functions, defined in Figs. 2(b) and 2(c), respectively.

photon fragmentation functions should be compensated by corresponding differences in the perturbatively calculated hard parts [20,21]. In principle, all consistent renormalization schemes, such as the minimum subtraction (MS) or the modified minimum subtraction ( $\overline{\text{MS}}$ ) scheme, are all equivalent for calculating the fragmentation functions. However, because the MS and  $\overline{\text{MS}}$  schemes are not necessary to respect the mass threshold, the virtual photon fragmentation functions calculated in these schemes can be negative [31]. In this paper, we introduce a new invariant mass cutoff scheme, which not only systematically remove the ultraviolet (UV) divergences associated with the composite operators, but also give a clear physical intuition to the fragmentation functions. The virtual photon fragmentation functions derived in this scheme respect the mass threshold constraints and can be positive definite.

In order to be consistent with the approximations that we used to derive the factorized formula in Eq. (5), the virtual photon fragmentation functions defined in Eqs. (8) and (9)

should only include the leading logarithmic contributions from the cut-vertex diagrams in Fig. 3. In order to extract the leading logarithmic contributions, we need to assume the strong ordering in the fragmenting partons' invariant masses,  $k_{i+1}^2 \gg k_i^2$ , as shown in Fig. 4(a). Since we are only interested in the resummation of the leading logarithmic contributions into the virtual photon fragmentation functions, the strong ordering in the partons' invariant masses is effectively the same as the familiar strong ordering in the partons' transverse momenta. In order to take into account the mass threshold effect due to the nonvanishing  $Q^2$ , we keep the type-II power corrections of  $O(Q^2/k_0^2)$  for the quark-to-virtual-photon splitting with  $k_0$  defined in Fig. 4(a). As defined in Ref. [17], the type-II power corrections correspond to the power corrections to the evolution equations while the type-I power corrections are the corrections directly to the physical observables, such as cross sections.

With the approximation of the strong ordering in the partons' invariant masses, only the ladder cut-vertex diagrams,

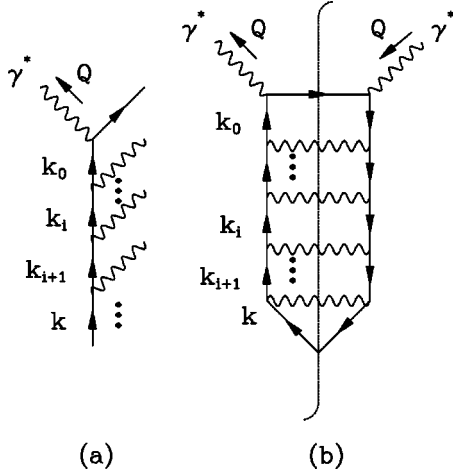


FIG. 4. (a) A sample decay amplitude for a virtual quark of invariant mass  $k^2$  to a virtual photon of invariant mass  $Q^2$ ; (b) corresponding ladder cut-vertex diagram contributed to the quark-to-virtual-photon fragmentation.

as shown in Fig. 4(b) as well as those in Fig. 3, contribute to the virtual photon fragmentation functions. After taking care of the renormalization of the elementary divergent diagrams in QCD and QED, only UV divergences left in the ladder cut-vertex diagrams are from the skeleton ladder cut-vertex diagrams and those associated with the wave function renormalization of the fields in the composite operators (or at the cut vertices). If we fix the wave function renormalization of these parton fields in the same way that we renormalize QCD Lagrangian, a cutoff on the parent parton's invariant mass  $k^2 \leq \mu_F^2$ , as shown in Fig. 3 or in Fig. 4, can remove all UV divergences of the skeleton ladder cut-vertex diagrams. Therefore, the virtual photon fragmentation functions defined with such an invariant mass cutoff scheme are perturbatively finite to all orders in  $\alpha_s$ . Since the different renormalization conditions result into the finite differences in the virtual photon fragmentation functions, we conclude that the virtual photon fragmentation functions defined above are perturbatively calculable.

The finiteness of the virtual photon fragmentation functions, defined with an invariant mass cutoff scheme, is most apparent if one identifies the fragmentation function  $D_{f \rightarrow \gamma^*}(z, \mu_F^2; Q^2)$  as the leading logarithmic contributions to the inclusive decay rate for a parton of invariant mass  $\mu_F$  and flavor  $f$  to a virtual photon of invariant mass  $Q$ . If  $Q \gg \Lambda_{\text{QCD}}$ , such inclusive decay rate is free of the collinear divergence and is perturbatively calculable. In addition, such inclusive decay rate can be positive definite with a proper choice of the wave function renormalization for the “decaying” parton  $f$ .

### B. Lowest order virtual photon fragmentation functions

In order to evaluate the virtual photon fragmentation functions  $D_{f \rightarrow \gamma^*}(z, \mu_F^2; Q^2)$ , we need to specify the polarization vector  $\epsilon_\lambda^\mu(Q)$  for the virtual photon state  $|\gamma^*(Q)\rangle$ . For an unpolarized virtual photon, we need only the following polarization tensor

$$P^{\mu\nu}(Q) \equiv \sum_{\lambda=T,L} \epsilon_\lambda^{\mu*}(Q) \epsilon_\lambda^\nu(Q), \quad (10)$$

where  $T$  and  $L$  represent the virtual photon's transverse and longitudinal polarization, respectively. Although the fragmentation functions defined in Eqs. (8) and (9) are gauge invariant, the functional form of the polarization tensor  $P^{\mu\nu}(Q)$  as well as the number of Feynman diagrams contributing to the fragmentation functions are gauge dependent.

In the light-cone gauge, we have the polarization tensor

$$P^{\mu\nu}(Q) = -g^{\mu\nu} + \frac{Q^\mu n^\nu + n^\mu Q^\nu}{Q \cdot n}, \quad (11)$$

and have only one Feynman diagram, as shown in Fig. 2(d), which contributes to the lowest order quark-to-virtual-photon fragmentation function. With an invariant mass cutoff on the fragmenting parton  $k^2 \leq \mu_F^2$  and a kinematic mass threshold  $k^2 \geq Q^2/z$ , we obtain the lowest order quark-to-virtual-photon fragmentation function:

$$D_{q \rightarrow \gamma^*}^{(0)}(z, \mu_F^2; Q^2) = e_q^2 \left( \frac{\alpha_{em}}{2\pi} \right) \left[ \left( \frac{1 + (1-z)^2}{z} \right) \ln \left( \frac{z\mu_F^2}{Q^2} \right) - z \left( 1 - \frac{Q^2}{z\mu_F^2} \right) \right], \quad (12)$$

where  $e_q$  is the fractional charge for the quark of flavor  $q$ . The fragmentation function,  $D_{q \rightarrow \gamma^*}^{(0)}(z, \mu_F^2; Q^2) \rightarrow 0$  as  $\mu_F^2$  approaches the mass threshold  $Q^2/z$ .

In principle, one could choose the fragmentation scale  $\mu_F^2$  to be less than  $Q^2/z$ , and consequently, the virtual photon fragmentation functions become negative. This freedom is a consequence of the fact that the fragmentation functions are not the directly measured physical quantities. However, in any consistent calculations of the physically measured quantities, such as the cross sections, this freedom should not affect our predictions. Just like the different choices of the renormalization schemes, the finite differences in the fragmentation functions, due to the different choices of the  $\mu_F$ , are compensated by corresponding differences in the perturbatively calculated short-distance parts [20]. In the rest of this paper, we respect the mass threshold and choose the  $\mu_F^2 \geq Q^2/z$ .

For an arbitrary choice of gauge, we need a total of four Feynman diagrams for calculating the lowest order quark-to-virtual-photon fragmentation function, as shown in Fig. 5 [30,31]. The diagrams in Fig. 5 contain the “eikonal” lines, which are labeled by the double solid lines. The Feynman rules for the “eikonal” lines can be found in Refs. [23,30]. These four diagrams in Fig. 5 form a gauge invariant set at this order [30,31]. Contributions of the three diagrams from Figs. 5(b)–5(d) vanish when they are contracted by the light-cone gauge polarization tensor in Eq. (11). By using the covariant polarization tensor

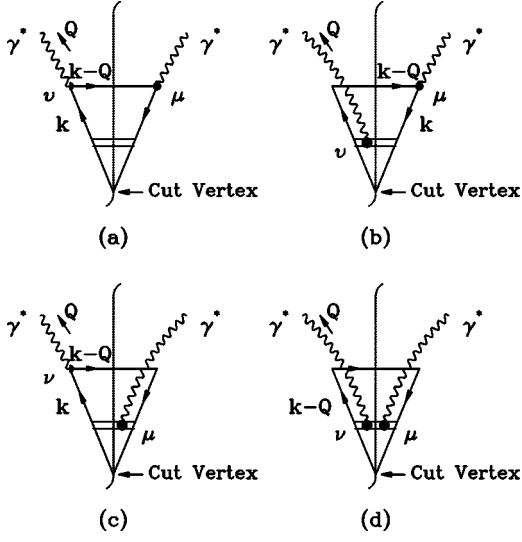


FIG. 5. Lowest order gauge invariant set of Feynman diagrams for quark-to-virtual-photon fragmentation functions [30].

$$P^{\mu\nu}(Q) = -g^{\mu\nu} + \frac{Q^\mu Q^\nu}{Q^2}, \quad (13)$$

or simply  $P^{\mu\nu}(Q) = -g^{\mu\nu}$ , we calculate the lowest order quark-to-virtual photon fragmentation function with the four diagrams in Fig. 5, and obtain the same fragmentation function given in Eq. (12). Since gluon does not directly couple to a photon, the lowest order gluon-to-virtual-photon fragmentation function vanishes:

$$D_{g \rightarrow \gamma^*}^{(0)}(z, \mu_F^2; Q^2) = 0. \quad (14)$$

### C. Virtual photon fragmentation functions with all order resummation

In order to generalize our calculations in Sec. II B to all orders in  $\alpha_s$ , we rewrite the lowest order quark-to-virtual-photon fragmentation function in Eq. (12) as follows:

$$D_{q \rightarrow \gamma^*}^{(0)}(z, \mu_F^2; Q^2) = \int_{Q^2/z}^{\mu_F^2} \frac{dk^2}{k^2} \left( \frac{\alpha_{em}}{2\pi} \gamma_{q \rightarrow \gamma^*}^{(0)}(z, k^2; Q^2) \right) \quad (15)$$

with

$$\gamma_{q \rightarrow \gamma^*}^{(0)}(z, k^2; Q^2) = e_q^2 \left[ \frac{1 + (1-z)^2}{z} - z \left( \frac{Q^2}{zk^2} \right) \right] \theta \left( k^2 - \frac{Q^2}{z} \right), \quad (16)$$

where the  $\theta$  function is a result of our choice to respect the mass threshold. By applying  $\mu_F^2 d/d\mu_F^2$  to both sides in Eq. (15), we obtain the evolution equation of the lowest order quark-to-virtual-photon fragmentation function

$$\mu_F^2 \frac{d}{d\mu_F^2} D_{q \rightarrow \gamma^*}^{(0)}(z, \mu_F^2; Q^2) = \left( \frac{\alpha_{em}}{2\pi} \right) \gamma_{q \rightarrow \gamma^*}^{(0)}(z, \mu_F^2; Q^2). \quad (17)$$

We identify the  $(\alpha_{em}/2\pi) \gamma_{q \rightarrow \gamma^*}^{(0)}$  in the right-hand side of Eq. (17) as the lowest order quark-to-virtual-photon evolution kernel of the evolution equation.

To illustrate the resummation to all orders in  $\alpha_s$ , we consider the nonsinglet contributions to the quark-to-virtual-photon fragmentation function. Under the approximation of the strong ordering in the partons' invariant masses, the leading logarithmic contributions to the nonsinglet quark-to-virtual-photon fragmentation function are given by the ladder cut-vertex diagrams shown in Fig. 3(b) plus those with the proper insertions of wave function renormalization of the quark fields. The leading logarithmic contributions from these ladder diagrams can be resummed to all orders in  $\alpha_s$ , [27],

$$\begin{aligned} D_{q \rightarrow \gamma^*}^{NS}(z, \mu_F^2; Q^2) &= \int_{Q^2/z}^{\mu_F^2} \frac{dk_0^2}{k_0^2} \left( \frac{\alpha_{em}}{2\pi} \gamma_{q \rightarrow \gamma^*}^{(0)}(z, k_0^2; Q^2) \right) \\ &+ \sum_{n=1}^{\infty} \left\{ \prod_{i=1}^n \int_{Q^2/z}^{k_{i+1}^2} \frac{dk_i^2}{k_i^2} \left[ \frac{\alpha_s}{2\pi} \int_{z_{i+1}}^1 \frac{dz_i}{z_i} P_{q \rightarrow q}^{(0)} \left( \frac{z_{i+1}}{z_i} \right) \right] \right\} \\ &\times \int_{Q^2/z}^{k_1^2} \frac{dk_0^2}{k_0^2} \left( \frac{\alpha_{em}}{2\pi} \gamma_{q \rightarrow \gamma^*}^{(0)}(z_1, k_0^2; Q^2) \right) \\ &= \int_{Q^2/z}^{\mu_F^2} \frac{dk_0^2}{k_0^2} \left( \frac{\alpha_{em}}{2\pi} \gamma_{q \rightarrow \gamma^*}^{(0)}(z, k_0^2; Q^2) \right) \\ &+ \int_{Q^2/z}^{\mu_F^2} \frac{dk^2}{k^2} \left[ \frac{\alpha_s}{2\pi} \int_z^1 \frac{dz'}{z'} P_{q \rightarrow q}^{(0)} \left( \frac{z}{z'} \right) \right] D_{q \rightarrow \gamma^*}^{NS}(z', k^2; Q), \end{aligned} \quad (18)$$

where the superscript “NS” represents the nonsinglet contributions, and the quark-to-quark evolution kernel  $P_{q \rightarrow q}^{(0)}(z)$  is the same as the leading order quark-to-quark evolution kernel of the DGLAP equations [27]. In Eq. (18), the integration limit,  $k_{n+1}^2 = \mu_F^2$ . By applying  $\mu_F^2 d/d\mu_F^2$  to both sides of Eq. (18), we obtain the leading order evolution equation for the nonsinglet quark-to-virtual-photon fragmentation function

$$\begin{aligned} \mu_F^2 \frac{d}{d\mu_F^2} D_{q \rightarrow \gamma^*}^{NS}(z, \mu_F^2; Q^2) &= \frac{\alpha_{em}}{2\pi} \gamma_{q \rightarrow \gamma^*}^{(0)}(z, \mu_F^2; Q^2) \\ &+ \frac{\alpha_s}{2\pi} \int_z^1 \frac{dz'}{z'} P_{q \rightarrow q}^{(0)} \left( \frac{z}{z'} \right) D_{q \rightarrow \gamma^*}^{NS}(z', \mu_F^2; Q^2). \end{aligned} \quad (19)$$

Because quark can interact directly with the virtual photon, the evolution equation for the quark-to-virtual-photon fragmentation function in Eq. (19) has an inhomogeneous term. From Eq. (16), the evolution kernel for the inhomogeneous

term has a type-II power correction term  $O(Q^2/\mu_F^2)$ . As discussed in the next section, such a power correction is very important near the mass threshold. It strongly suppresses the evolution of the fragmentation function to a *transversely* polarized virtual photon in the threshold region, and it is necessary for resumming the large logarithmic contributions to the production of a *longitudinally* polarized virtual photon. In a contrary, the effect of such power correction  $O(Q^2/\mu_F^2)$  to the virtual photon structure functions (the spacelike counterpart of the virtual photon fragmentation functions) should be less dramatic due to the difference in the mass threshold when the virtual photon is analytically continued from timelike to spacelike [18,19].

Following the arguments given in Ref. [28], we generalize the derivation of Eq. (19) to derive the evolution equations for the singlet quark-to-virtual-photon and gluon-to-virtual-photon fragmentation functions, and we obtain

$$\begin{aligned} \mu_F^2 \frac{d}{d\mu_F^2} D_{c \rightarrow \gamma^*}(z, \mu_F^2; Q^2) &= \left( \frac{\alpha_{em}}{2\pi} \right) \gamma_{c \rightarrow \gamma^*}(z, \mu_F^2, \alpha_s; Q^2) \\ &+ \left( \frac{\alpha_s}{2\pi} \right) \sum_d \int_z^1 \frac{dz'}{z'} P_{c \rightarrow d} \left( \frac{z}{z'}, \alpha_s \right) D_{d \rightarrow \gamma^*}(z', \mu_F^2; Q^2), \end{aligned} \quad (20)$$

where  $c, d = q, \bar{q}, g$ . The evolution kernels  $\gamma_{c \rightarrow \gamma^*}$  and  $P_{c \rightarrow d}$  in Eq. (20) have the following perturbative expansions:

$$\gamma_{c \rightarrow \gamma^*}(z, \mu_F^2, \alpha_s; Q^2) = \sum_{n=0} \gamma_{c \rightarrow \gamma^*}^{(n)}(z, \mu_F^2; Q^2) \left( \frac{\alpha_s}{2\pi} \right)^n, \quad (21)$$

$$P_{c \rightarrow d}(z, \alpha_s) = \sum_{n=0} P_{c \rightarrow d}^{(n)}(z) \left( \frac{\alpha_s}{2\pi} \right)^n, \quad (22)$$

where the renormalization scale dependence is suppressed. With the strong ordering approximation in the partons' invariant masses, the evolution kernels  $P_{c \rightarrow d}$  for the homogeneous terms in Eq. (20) are the same as that for the evolution equations of the real photon (or other single hadron) fragmentation functions, which are also the same as the evolution kernels of the DGLAP equations [27,29]. In this paper, we keep the power corrections due to the mass threshold only at the last quark-to-virtual-photon splitting, and neglect all high order inhomogeneous terms  $\gamma_{c \rightarrow \gamma^*}^{(n \geq 1)}$  in Eq. (21). As discussed above, even the lowest order evolution kernels  $\gamma_{c \rightarrow \gamma^*}^{(0)}$  depend on the renormalization conditions of the cut vertices. In terms of the invariant mass cutoff scheme defined above, the lowest order quark-to-virtual-photon evolution kernel is given in Eq. (16), and the lowest order gluon-to-virtual-photon evolution kernel vanishes,

$$\gamma_{g \rightarrow \gamma^*}^{(0)}(z, \mu_F^2; Q^2) = 0. \quad (23)$$

The all-order resummation of the large logarithms into the virtual photon fragmentation functions are achieved by solving the evolution equations in Eq. (20). Although the evolution equations for the virtual photon fragmentation functions have the same functional forms as that for the real photon fragmentation functions [4], the nonvanishing  $Q^2$  and the different inhomogeneous terms lead to many differences between the real and virtual photon fragmentation functions. In particular, the virtual photon fragmentation functions provide the systematically resummed contributions to a longitudinally polarized virtual photon. With the lowest order evolution kernels  $\gamma_{q \rightarrow \gamma^*}^{(0)}$  in Eq. (16) and  $P_{c \rightarrow d}^{(0)}$  from Ref. [29], we solve the evolution equations in Eq. (20) for the unpolarized virtual photon fragmentation functions, and present the numerical results in Sec. IV.

### III. POLARIZED VIRTUAL PHOTON FRAGMENTATION FUNCTIONS

By measuring the momenta of both leptons in Drell-Yan massive lepton-pair production, we can determine both invariant mass and polarization state of the virtual photon, which decays into the lepton pair. Therefore, it is meaningful to define the fragmentation functions to a polarized virtual photon. In this section, we calculate the evolution kernels for the evolution equations of polarized virtual photon fragmentation functions.

Since we did not use any constraints due to the virtual photon's polarization when we derived the cut-vertex and operator definitions for the virtual photon fragmentation functions in last section, the same definitions should be valid for fragmentation functions to a polarized virtual photon. Therefore, with a proper choice of polarization vectors  $\epsilon_\lambda^\mu(Q)$  for a virtual photon of polarization  $\lambda$ , we can calculate the fragmentation functions to a virtual photon of a specific polarization state.

In order to specify a polarized virtual photon state, we need to define the photon's polarization vector  $\epsilon_\lambda^\mu(Q)$ . If the photon is real ( $Q^2=0$ ), it has only *two* transverse polarization states and its longitudinal polarization can be gauged away by an extra gauge transformation. When the photon is virtual and its quantum numbers are completely fixed by the physical observables, the extra gauge degree of freedom used to remove the longitudinal polarization at  $Q^2=0$  is lost, and therefore, the virtual photon has three polarization states.

With our choice of the frame in which the virtual photon is moving very fast along the  $z$  axis, we define the photon's polarization vectors as

$$\begin{aligned} \epsilon_{T=1}^\mu(Q) &= (0^+, 0^-, 1, 0), \\ \epsilon_{T=2}^\mu(Q) &= (0^+, 0^-, 0, 1), \\ \epsilon_L^\mu(Q) &= \frac{1}{Q} (Q^+, -Q^-, \vec{0}_T), \end{aligned} \quad (24)$$

which are effectively the same as those in the ‘‘S-helicity’’ frame defined in Ref. [32]. We obtain corresponding polarization tensors,

$$P_T^{\mu\nu}(Q) \equiv \frac{1}{2} \sum_{T=1,2} \epsilon_T^{*\mu}(Q) \epsilon_T^\nu(Q) = \frac{1}{2} d^{\mu\nu} \quad (25)$$

with  $d^{\mu\nu}$  defined in Eq. (7) and

$$P_L^{\mu\nu}(Q) \equiv \epsilon_L^{*\mu}(Q) \epsilon_L^\nu(Q) \quad (26)$$

for transversely and longitudinally polarized virtual photons, respectively. By summing over all polarization states, we should recover the polarization tensor for an unpolarized virtual photon

$$P^{\mu\nu}(Q) = 2P_T^{\mu\nu}(Q) + P_L^{\mu\nu}(Q), \quad (27)$$

where the factor of 2 represents the virtual photon's two transverse polarization states.

Applying the transverse polarization tensor  $P_T^{\mu\nu}$  to the lowest order Feynman diagrams in Fig. 5, we obtain the lowest order fragmentation function for a quark to a transversely polarized virtual photon as

$$D_{q \rightarrow \gamma_T^*}^{(0)}(z, \mu_F^2; Q^2) = e_q^2 \left( \frac{\alpha_{em}}{2\pi} \right) \frac{1}{2} \left( \frac{1+(1-z)^2}{z} \right) \times \left[ \ln \left( \frac{z\mu_F^2}{Q^2} \right) - \left( 1 - \frac{Q^2}{z\mu_F^2} \right) \right] \quad (28)$$

with  $\mu_F^2 \geq Q^2/z$ . Again, the lowest order fragmentation function for a gluon to a photon vanishes,  $D_{g \rightarrow \gamma_T^*}^{(0)}(z, \mu_F; Q) = 0$ . Corresponding evolution kernels are given by

$$\begin{aligned} \gamma_{q \rightarrow \gamma_T^*}^{(0)}(z, \mu_F^2; Q^2) &= e_q^2 \frac{1}{2} \left( \frac{1+(1-z)^2}{z} \right) \\ &\times \left[ 1 - \frac{Q^2}{z\mu_F^2} \right] \theta \left( \mu_F^2 - \frac{Q^2}{z} \right), \\ \gamma_{g \rightarrow \gamma_T^*}^{(0)}(z, \mu_F^2; Q^2) &= 0. \end{aligned} \quad (29)$$

As expected, when  $Q \rightarrow 0$ ,  $2\gamma_{q \rightarrow \gamma_T^*}^{(0)}$  in Eq. (29) reduces to the lowest order evolution kernels for the real photon fragmentation functions [4].

Similarly, by applying the longitudinal polarization tensor  $P_L^{\mu\nu}$  in Eq. (26) to the Feynman diagrams in Fig. 5, we derive

$$D_{q \rightarrow \gamma_L^*}^{(0)}(z, \mu_F^2; Q^2) = e_q^2 \left( \frac{\alpha_{em}}{2\pi} \right) \left[ 2 \left( \frac{1-z}{z} \right) \right] \left( 1 - \frac{Q^2}{z\mu_F^2} \right), \quad (30)$$

with  $\mu_F^2 \geq Q^2/z$ , and  $D_{g \rightarrow \gamma_L^*}^{(0)}(z, \mu_F^2; Q^2) = 0$ . The  $(1-z)$  factor in Eq. (30) is a consequence of the vector interaction between the quark and photon. As a consistency check, our lowest order polarized virtual photon fragmentation functions in Eqs. (28) and (30) satisfy

$$\begin{aligned} &2D_{q \rightarrow \gamma_T^*}^{(0)}(z, \mu_F^2; Q^2) + D_{q \rightarrow \gamma_L^*}^{(0)}(z, \mu_F^2; Q^2) \\ &= D_{q \rightarrow \gamma^*}^{(0)}(z, \mu_F^2; Q^2), \end{aligned} \quad (31)$$

where  $D_{q \rightarrow \gamma^*}^{(0)}$  is given in Eq. (12). From Eq. (30), we derive the evolution kernels for longitudinally polarized virtual photon fragmentation functions

$$\begin{aligned} \gamma_{q \rightarrow \gamma_L^*}^{(0)}(z, \mu_F^2; Q^2) &= e_q^2 \left[ 2 \left( \frac{1-z}{z} \right) \right] \left( \frac{Q^2}{z\mu_F^2} \right) \theta \left( \mu_F^2 - \frac{Q^2}{z} \right), \\ \gamma_{g \rightarrow \gamma_L^*}^{(0)}(z, \mu_F^2; Q^2) &= 0. \end{aligned} \quad (32)$$

Again, we have  $2\gamma_{q \rightarrow \gamma_T^*}^{(0)} + \gamma_{q \rightarrow \gamma_L^*}^{(0)} = \gamma_{q \rightarrow \gamma^*}^{(0)}$ .

Since the polarized evolution kernels and the polarized virtual photon fragmentation functions are gauge invariant, we can also derive them from the single diagram in Fig. 2(d) in the light-cone gauge. Substituting  $Q^\mu = Q^+ \bar{n}^\mu + Q^- n^\mu$  into the polarization tensor in the light-cone gauge in Eq. (11), we obtain

$$P^{\mu\nu}(Q) = d^{\mu\nu} + \frac{Q^2}{(Q^+)^2} n^\mu n^\nu. \quad (33)$$

Since the vector  $n^\mu$  used to fix the light-cone gauge does not have transverse component, the  $d^{\mu\nu}$  in Eq. (33) should still be identified as  $2P_T^{\mu\nu}(Q)$ . From Eq. (27), we obtain the effective polarization tensor for a longitudinally polarized virtual photon

$$P_L^{\mu\nu}(Q) = \frac{Q^2}{(Q^+)^2} n^\mu n^\nu \quad (34)$$

in the light-cone gauge. Applying this  $P_L^{\mu\nu}(Q)$  to the Feynman diagram in Fig. 2(d), we can derive the lowest order fragmentation functions to a longitudinally polarized virtual photon. As expected, the derived fragmentation functions are the same as those given in Eq. (30).

Since the fragmentation functions to a polarized and an unpolarized virtual photon share the same form of the operator definitions, the evolution equations for polarized virtual photon fragmentation functions have the same functional form as that in Eq. (20), except the evolution kernels  $\gamma_{c \rightarrow \gamma^*}$  are replaced by those in Eq. (29) and Eq. (32) for transversely polarized and longitudinally polarized virtual photon, respectively. Since the evolution kernels  $P_{c \rightarrow d}$  are independent of the polarization of the produced virtual photon, they should remain the same.

#### IV. NUMERICAL RESULTS AND CONCLUSIONS

In the last two sections, we derived the analytical expressions for the lowest order parton-to-virtual-photon fragmentation functions with the virtual photon unpolarized as well as polarized. The lowest order gluon-to-virtual-photon fragmentation functions vanish while the lowest order quark-to-

virtual-photon fragmentation functions are given in Eqs. (12), (28), and (30) for unpolarized, transversely polarized, and longitudinally polarized, respectively. Strong interactions in the top blob of the cut-vertex diagrams in Figs. 2(b) and 2(c) can change the  $z$  as well as the  $\mu_F$  dependence of the lowest order virtual photon fragmentation functions. Solving the evolution equations in Eq. (20) is effectively to resum all leading logarithmic contributions from the strong interactions.

In order to solve the evolution equations in Eq. (20), we need to specify a boundary condition. Unlike the real photon fragmentation functions, we do not need any nonperturbative input distributions if the invariant mass  $Q \gg \Lambda_{\text{QCD}}$ . From the mass threshold constraints, we have the following boundary condition for solving the evolution equations in Eq. (20):

$$D_{f \rightarrow \gamma^*}(z, \mu_F^2 = Q^2/z; Q^2) = 0 \quad (35)$$

for all parton flavor  $f = q, \bar{q}, g$  and any polarization of the virtual photon.

Since the boundary conditions given in Eq. (35) are the same for all flavors of massless partons, and the evolution kernels  $\gamma_{c \rightarrow \gamma^*}^{(0)}$  in Eq. (20) are the same for a quark  $q$  and corresponding antiquark  $\bar{q}$ , we have

$$D_{q \rightarrow \gamma^*}(z, \mu_F^2; Q^2) = D_{\bar{q} \rightarrow \gamma^*}(z, \mu_F^2; Q^2) \quad (36)$$

for all quark flavor  $q$ . By neglecting the quark mass difference, the only flavor dependence of the evolution kernels  $\gamma_{c \rightarrow \gamma^*}^{(0)}$  in Eq. (20) is from quark's fractional charge  $e_q$ . Therefore, the quark-to-virtual-photon fragmentation functions are the same for all quark flavors with the same fractional charge.

With the boundary condition given in Eq. (35), we can solve the evolution equations in Eq. (20) in the moment space analytically, and then, perform the Mellin transformation from the moment space back to the  $z$  space [4]. However, we find that it is easier to solve the evolution equations numerically in the  $z$  space directly.

In Figs. 6(a) and 6(b), we plot the derived lowest order quark-to-virtual-photon fragmentation functions as a function of the momentum fraction  $z$  at a fragmentation scale  $\mu_F = 10$  GeV and  $\mu_F = 50$  GeV, respectively. We choose  $e_q = 2/3$  for the quark's fractional charge, and the virtual photon's invariant mass to be  $Q = 5$  GeV. The unpolarized quark-to-virtual-photon fragmentation functions given in Eq. (12) are represented by the solid lines. The transversely and longitudinally polarized virtual photon fragmentation functions given in Eqs. (28) and (30) are represented by the dashed and dotted lines, respectively. The solid lines are equal to twice of the dashed lines plus the dotted lines, which is a consequence of Eq. (31). Notice that other than the longitudinal case, the lowest order virtual photon fragmentation functions do not vanish as  $z \rightarrow 1$ . However, as explained below, this feature is an artifact of the lowest order calculations.

From Fig. 6, we find that longitudinally polarized virtual photon fragmentation functions are much larger than the transversely polarized virtual photon fragmentation functions

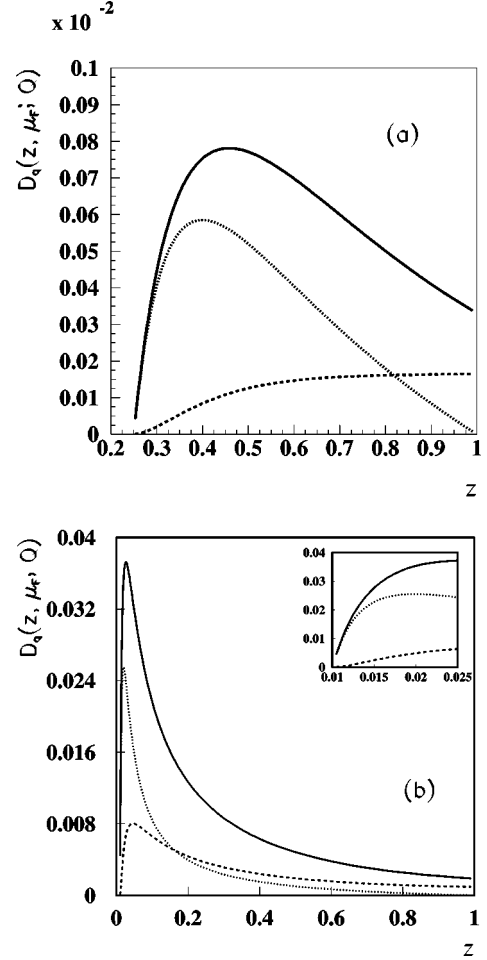


FIG. 6. The lowest order virtual photon fragmentation functions as a function of  $z$  at  $Q = 5$  GeV and  $\mu_F = 10$  GeV (a) and  $\mu_F = 50$  GeV (b). The solid, dashed, and dotted lines are for unpolarized, transversely polarized, and longitudinally polarized virtual photons, respectively. The inset in Fig. 2(b) shows the  $z \leq 0.025$  region.

when  $z$  is small. The small  $z$  region corresponds to the region where  $\mu_F^2$  is close to the threshold  $Q^2/z$ . Near the threshold, the evolution kernels for the transversely polarized fragmentation functions  $\gamma_{q \rightarrow \gamma_T^*}(0)$  in Eq. (29) vanish while the kernels for the longitudinally polarized fragmentation functions  $\gamma_{q \rightarrow \gamma_L^*}^{(0)}$  in Eq. (32) are finite and large. The  $\gamma_{q \rightarrow \gamma_L^*}^{(0)}$  are actually proportional to  $1/z$  when  $\mu_F^2 \rightarrow Q^2/z$ . Therefore, the longitudinally polarized virtual photon fragmentation functions dominate the small  $z$  or the threshold region.

On the other hand, the fragmentation functions for a transversely polarized virtual photon evolve much faster than the longitudinally polarized fragmentation functions in the large  $z$  region, as shown in Fig. 6. This is because the evolution kernels  $\gamma_{q \rightarrow \gamma_L^*}^{(0)}$  for the longitudinally polarized virtual photon fragmentation functions are power suppressed (proportional to  $1/\mu_F^2$ ) and also vanish as  $z \rightarrow 1$ .

In order to see the effect of the large logarithmic contributions from QCD strong interactions, we numerically solve the evolution equations in Eq. (20) with the lowest order

evolution kernels  $\gamma_{q \rightarrow \gamma^*}^{(0)}$  and  $P_{c \rightarrow d}^{(0)}$ . As shown in Ref. [27], both QCD evolution kernels,  $P_{q \rightarrow q}^{(0)}(z)$  and  $P_{g \rightarrow g}^{(0)}(z)$ , have the  $1/(1-z)_+$  dependence. Because of this  $1/(1-z)_+$  dependence, the right-hand-side of Eq. (20) has a term proportional to  $D_{c \rightarrow \gamma^*}(z, \mu_F^2; Q^2) \ln(1-z)$ , which approaches  $-\infty$  as  $z \rightarrow 1$  unless  $D_{c \rightarrow \gamma^*}(z \rightarrow 1, \mu_F^2; Q^2)$  vanishes faster than  $1/\ln(1-z)$ . From the boundary conditions in Eq. (35), we conclude that the QCD evolved virtual photon fragmentation functions  $D_{f \rightarrow \gamma^*}(z, \mu_F^2; Q^2)$  vanish at  $z=1$  for all parton flavor  $f=q, \bar{q}, g$ . Physically, when  $\mu_F^2 > Q^2$ , a virtual parton (quark or gluon) of invariant mass  $\mu_F$  should have a zero probability not to radiate any soft gluons before producing the virtual photon of invariant mass  $Q$ , and therefore, the probability density for a virtual photon to have the momentum fraction  $z=1$  should vanish.

We plot the comparison between the lowest order (dashed) and the QCD evolved (solid) quark-to-virtual-photon fragmentation functions at  $Q=5$  GeV and  $\mu_F=50$  GeV in Fig. 7(a).  $U$ ,  $T$ , and  $L$  represent the fragmentation functions to a unpolarized, transversely polarized, and longitudinally polarized virtual photon, respectively. As with the evolution of parton distributions, QCD evolution tries to enlarge the fragmentation functions in the small  $z$  region, and to suppress the fragmentation functions in the large  $z$  region. The difference between the QCD evolved and lowest order fragmentation functions at  $Q=5$  GeV is small because of the boundary conditions in Eq. (35). However, when  $Q$  is smaller or  $\mu_F$  is larger, we expect QCD evolution to be much more important because of a larger logarithm  $\ln(\mu_F^2/Q^2)$ . For example, cross sections for virtual photon production were measured by UA1 Collaboration at CERN for the virtual photon mass  $Q \in [2m_\mu, 2.5]$  GeV [33]. Instead of  $Q=5$  GeV in Fig. 7(a), we plot the same quark-to-virtual-photon fragmentation functions at  $Q=1.5$  GeV in Fig. 7(b). Clearly, QCD evolved virtual photon fragmentation functions in Fig. 7(b) are enhanced in comparison with those in Fig. 7(a), particularly, in the small  $z$  region. Our numerical results in Fig. 7 show that the inhomogeneous terms in the evolution equations in Eq. (20) dominate the evolution. Therefore, any high order corrections in  $\alpha_s$  and/or power corrections to the homogeneous terms in Eq. (20) should not significantly change our numerical results.

Although we do not have the lowest order gluon-to-virtual-photon fragmentation functions due to  $\gamma_{g \rightarrow \gamma^*}^{(0)}=0$ , QCD evolution in Eq. (20) can generate the gluon-to-virtual-photon fragmentation functions. In Figs. 8(a) and 8(b), we plot gluon-to-virtual-photon fragmentation functions at  $\mu_F=10$  GeV and  $\mu_F=50$  GeV, respectively. The virtual photon mass is again chosen to be  $Q=5$  GeV. As shown in Fig. 8, QCD evolution generated gluon-to-virtual-photon fragmentation functions at  $Q=5$  GeV grow very fast when the fragmentation scale  $\mu_F^2$  increases. They are about two orders of magnitude smaller than the quark-to-virtual-photon fragmentation functions at  $\mu_F=10$  GeV, and only one order of magnitude smaller at  $\mu_F=50$  GeV. Therefore, at  $Q=1.5$  GeV or at a larger value of  $\mu_F$ , QCD generated gluon-to-virtual-photon fragmentation functions become more important.

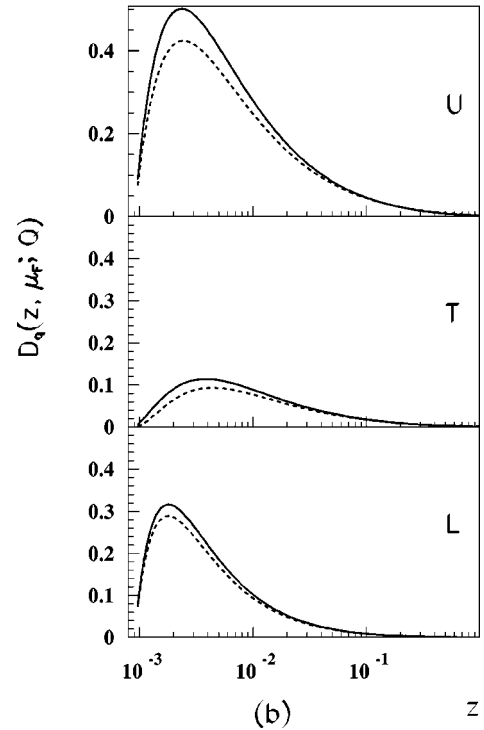
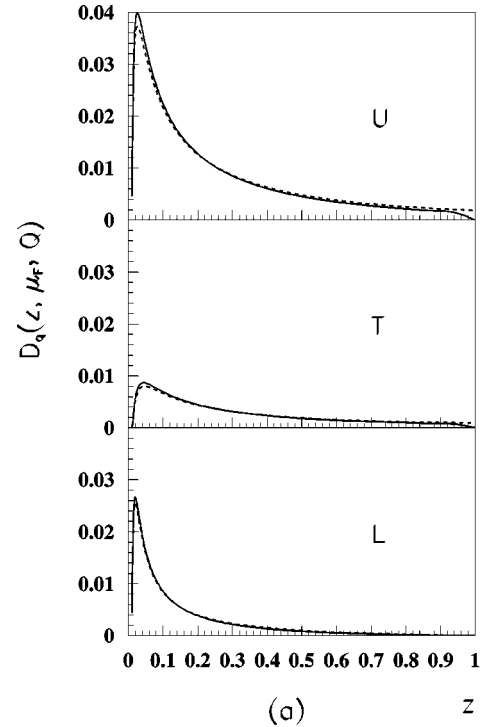


FIG. 7. Comparison between the lowest order (dashed) and the QCD evolved (solid) virtual photon fragmentation functions as a function of  $z$  at  $\mu_F=50$  GeV and  $Q=5$  GeV (a) and  $Q=1.5$  GeV (b).

In conclusion, we have argued that virtual photon fragmentation functions are well defined and physically meaningful. We derive the evolution equations for virtual photon fragmentation functions, and show that these fragmentation functions are perturbatively calculable. We demonstrate that

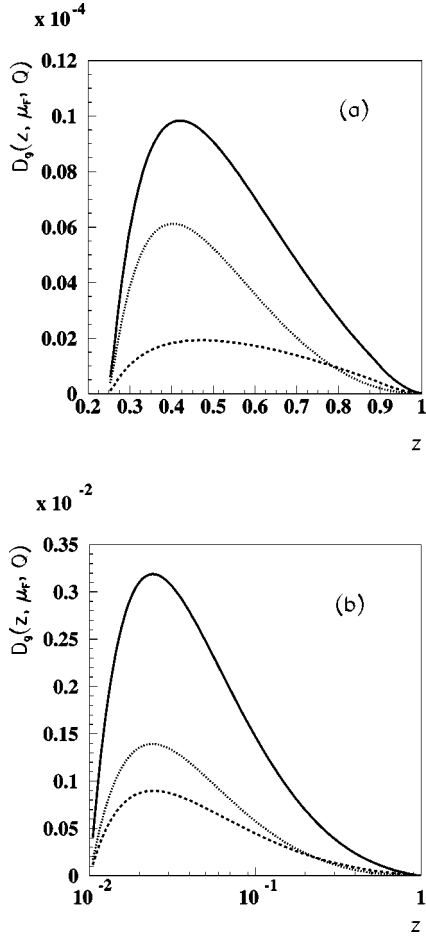


FIG. 8. QCD generated gluon-to-virtual-photon fragmentation functions as a function of  $z$  at  $Q=5$  GeV and  $\mu_F=10$  GeV (a), and  $\mu_F=50$  GeV (b). The solid, dashed, and dotted lines are for unpolarized, transversely polarized, and longitudinally polarized virtual photons, respectively.

QCD resummation of the large logarithms caused by quark and gluon radiation provides a very important contribution to the fragmentation functions when the fragmentation scale  $\mu_F$  is large and/or the invariant mass  $Q$  is relatively small. Just like pion fragmentation functions [4], the virtual photon fragmentation functions derived here are universal and can be applied to any processes with massive lepton-pair production. In the rest of this paper, we discuss some potential applications of our results.

Contributions of fragmentation functions  $D(z)$  to the physical observables generally depend on the production of the parent partons at the same  $z$ . Since the cross sections for producing the parent partons strongly depend on the momenta of the produced partons, the role of the fragmentation functions may be different for different regions of the  $z$  values. For example, for the Drell-Yan production, if the cross section is dominated by the small  $z$  region, the produced virtual photons will likely be longitudinally polarized. On the other hand, if the cross section is dominated by the large  $z$  region, the virtual photon will be transversely polarized. For a fixed collision energy  $\sqrt{S}$ , the Drell-Yan cross sections depend on the  $z$  value from  $z_{\min} = \sqrt{(Q^2 + Q_T^2)/S} [e^y + e^{-y}]$  to 1

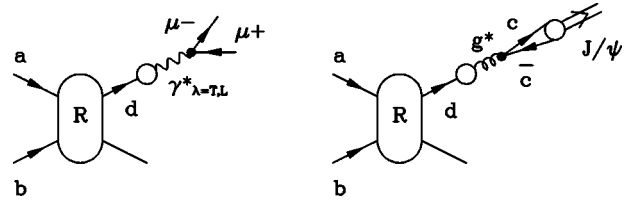


FIG. 9. Sketch for Drell-Yan massive lepton-pair and  $J/\psi$  production via parton fragmentation.

with the rapidity  $y$ . For  $Q=5$  GeV and  $y=0$  at  $\sqrt{S}=2$  TeV (the new Tevatron energy),  $z_{\min} \approx 0.01$  and  $0.05$  for  $Q_T=10$  and  $50$  GeV, respectively. It is clear from Fig. 6(b) that the produced virtual photons at  $Q_T \sim 50$  GeV are more likely to be transversely polarized. At  $Q_T=10$  GeV, the longitudinally polarized fragmentation functions in Fig. 6(a) are much larger than the transverse fragmentation functions in small  $z$  region, and the  $1/z^2$  factor in Eq. (5) for the convolution over  $z$  is also favor for producing a longitudinally polarized virtual photon. But, the cross section for producing a parent parton of momentum  $k_T$  at small  $z \approx Q_T/k_T$  is a very steep falling function of  $k_T$ , and consequently, it strongly reduces the rate for producing a longitudinally polarized virtual photon. In conclusion, when  $Q_T$  is large, the virtual photon produced in Drell-Yan massive lepton-pair production is more likely to be transversely polarized [21].

Recently, it was found that the  $J/\psi$  mesons produced at Fermilab Tevatron become more longitudinally polarized as the transverse momentum increases [22]. On the other hand, various theoretical calculations predict the  $J/\psi$  mesons to be more transversely polarized [34]. The virtual photon production (extracted from Drell-Yan massive lepton-pair production) at large  $Q_T$  and small  $Q^2$  has a lot in common with the  $J/\psi$  production at high  $Q_T$ . They both have two large physical scales:  $Q_T$  and  $Q^2$ , which is equal to  $M_{J/\psi}^2$  in the case of  $J/\psi$  production; and  $Q_T^2$  is much larger than  $Q^2$ . If the collision energy  $\sqrt{S}$  is large enough and the logarithm  $\ln(Q_T^2/Q^2)$  is so important that the resummed fragmentation contributions dominate the production cross sections, the virtual photon and  $J/\psi$  production will share the *same* partonic subprocesses, labeled by the  $R$  in Fig. 9. With their respected fragmentation functions, both the virtual photon and  $J/\psi$  production at high  $Q_T$  are perturbatively calculable [35]. As discussed above, the virtual photon fragmentation functions are completely perturbative, while the parton to  $J/\psi$  fragmentation functions involve final-state nonperturbative interactions. Therefore, only difference between the virtual photon and  $J/\psi$  production at high  $Q_T$  and large  $\sqrt{S}$  is the final-state strong interactions during the formation of  $J/\psi$  meson. We propose to measure the virtual photon polarization in Drell-Yan massive lepton-pair production at large  $Q_T$  and low  $Q^2$ . The measurements of the virtual photon's polarization at high  $Q_T$  provide not only a good test of QCD perturbation theory, but also a reference process to test the models of  $J/\psi$  formation.

As shown in Fig. 9, the fragmentation functions from a parton  $d$  to a physical  $J/\psi$  can be approximated by the fragmentation functions to a virtual gluon of invariant mass  $Q$ ,

which immediately decay into a  $c\bar{c}$  pair, convoluted with a transition from the  $c\bar{c}$  pair to a physical  $J/\psi$  [35]. Similar to the virtual photon fragmentation functions, the fragmentation functions for a parton to a virtual gluon (or the subsequent  $c\bar{c}$  pair) should be perturbatively calculable. But, the produced charm and anticharm quark pair of invariant mass  $Q$  can in principle radiate gluons and have soft interactions with other partons in the collisions. However, due to the heavy quark mass, such final-state interactions during the formation or transition from the produced  $c\bar{c}$  pair to a physical  $J/\psi$  meson are not expected to significantly change the polarization [34]. If the formation from the  $c\bar{c}$  pair of invariant mass  $Q$  to a physical  $J/\psi$  meson does not change the polarization, we could conclude that any polarization differences between the  $J/\psi$  meson and a virtual photon at large  $Q_T$  should only come from the possible differences between the fragmentation functions for a parton to a virtual gluon and to a virtual photon. Since the resummed contributions to a longitudinally polarized virtual gluon as well as a virtual photon are initiated by the power corrections  $O(Q^2/k_0^2)$  at the last splitting, as shown in Fig. 4, the produced virtual

gluons or virtual photons are more likely to be transversely polarized when  $\mu_F^2$  is much larger than  $Q^2$ . Therefore, one can expect the polarization of the  $J/\psi$  mesons produced at high  $Q_T$  to be similar to the polarization of the virtual photon in Drell-Yan massive lepton-pair production at the same kinematics, if the final-state  $J/\psi$  formation does not change the polarization. For example, the nonrelativistic QCD (NRQCD) model of  $J/\psi$  production predicts the  $J/\psi$  mesons to be transversely polarized at large transverse momentum [34], which is not consistent with recent Fermilab data [22]. Since the leptons do not interact strongly once produced, the measurements of the virtual photon polarization in Drell-Yan massive lepton-pair production at large transverse momentum should help us to narrow the questions about  $J/\psi$  production.

### ACKNOWLEDGMENTS

We thank G. Sterman for very helpful discussions. This work was supported in part by the U.S. Department of Energy under Grant No. DE-FG02-87ER40731.

- 
- [1] J. Huston *et al.*, Phys. Rev. D **58**, 114034 (1998).
  - [2] L. de Barbaro *et al.*, hep-ph/0006300, and references therein.
  - [3] S. Catani *et al.*, hep-ph/0005025, and references therein.
  - [4] J.F. Owens, Rev. Mod. Phys. **59**, 465 (1987).
  - [5] H. Baer, J. Ohnemus, and J.F. Owens, Phys. Rev. D **42**, 61 (1990).
  - [6] E.L. Berger and J.-W. Qiu, Phys. Lett. B **248**, 371 (1990); Phys. Rev. D **44**, 2002 (1991).
  - [7] P. Aurenche, R. Baier, and M. Fontannaz, Phys. Rev. D **42**, 1440 (1990); P. Aurenche *et al.*, Nucl. Phys. **B399**, 34 (1993); M. Glück, E. Reya, and A. Vogt, Phys. Rev. D **48**, 116 (1993); L. Bourhis, M. Fontannaz, and J.Ph. Guillet, Eur. Phys. J. C **2**, 529 (1998).
  - [8] H.L. Lai *et al.*, Eur. Phys. J. C **12**, 375 (2000).
  - [9] E.L. Berger, X.-F. Guo, and J.-W. Qiu, Phys. Rev. Lett. **76**, 2234 (1996); Phys. Rev. D **54**, 5470 (1996).
  - [10] A.D. Martin, R.G. Roberts, W.J. Stirling, and R.S. Thorne, Eur. Phys. J. C **4**, 463 (1998).
  - [11] L. Apanasevich *et al.*, Phys. Rev. D **59**, 074007 (1999).
  - [12] P. Aurenche *et al.*, Eur. Phys. J. C **9**, 107 (1999).
  - [13] E.L. Berger, L.E. Gordon, and M. Klasen, Phys. Rev. D **58**, 074012 (1998).
  - [14] J.C. Collins, D.E. Soper, and G. Sterman, in *Perturbative Quantum Chromodynamics*, edited by A. H. Mueller (World Scientific, Singapore, 1989).
  - [15] G.T. Bodwin, Phys. Rev. D **31**, 2616 (1985); **34**, 3932 (1986).
  - [16] J.C. Collins, D.E. Soper, and G. Sterman, Nucl. Phys. **B250**, 199 (1985).
  - [17] J.-W. Qiu and X.-F. Zhang, Phys. Rev. Lett. **86**, 2724 (2001); Phys. Rev. D **63**, 114011 (2001), and references therein.
  - [18] T. Uematsu and T.F. Walsh, Phys. Lett. **101B**, 263 (1981); Nucl. Phys. **B199**, 93 (1982).
  - [19] G. Rossi, UC-San Diego Report No. UCSD-10P10-227 (unpublished); G. Rossi, Phys. Rev. D **29**, 852 (1984).
  - [20] E.L. Berger, J.-W. Qiu, and X.-F. Zhang (in preparation).
  - [21] J.-W. Qiu, R. Rodriguez, and X.-F. Zhang, Phys. Lett. B **506**, 254 (2001).
  - [22] CDF Collaboration, T. Affolder *et al.*, Phys. Rev. Lett. **85**, 2886 (2000).
  - [23] J.C. Collins and D.E. Soper, Nucl. Phys. **B194**, 445 (1982).
  - [24] J. Qiu, Phys. Rev. D **42**, 30 (1990).
  - [25] A.H. Mueller, Phys. Rep. **73**, 237 (1981).
  - [26] We thank E. Braaten for pointing out the missing QED phase in an early preprint of this paper.
  - [27] J.C. Collins and J.-W. Qiu, Phys. Rev. D **39**, 1398 (1989).
  - [28] G. Curci, W. Furmanski, and R. Petronzio, Nucl. Phys. **B175**, 27 (1980).
  - [29] G. Sterman *et al.*, Rev. Mod. Phys. **67**, 157 (1995), and references therein.
  - [30] G.T. Bodwin and J.-W. Qiu, Phys. Rev. D **41**, 2755 (1990).
  - [31] E. Braaten and J. Lee (private communication).
  - [32] C.S. Lam and W.-K. Tung, Phys. Rev. D **18**, 2447 (1978).
  - [33] UA1 Collaboration, C. Albajar *et al.*, Phys. Lett. B **209**, 397 (1988).
  - [34] E. Braaten, B.A. Kniehl, and J. Lee, Phys. Rev. D **62**, 094005 (2000), and references therein.
  - [35] J.-W. Qiu and G. Sterman (in preparation).